

1 **Multi-Model Analysis of the Atmospheric Response to Antarctic Sea Ice Loss at**
2 **Quadrupled CO₂**

3 **H. C. Ayres¹, J. A. Screen¹**

4 ¹ College of Engineering, Mathematics and Physical Sciences, University of Exeter, Exeter EX4
5 4QE, UK.

6 Corresponding author: Holly Ayres (ha392@exeter.ac.uk)

7 **Key Points:**

- 8 • Projected Antarctic sea-ice loss weakens the tropospheric westerly jet and favors the
9 negative phase of the Southern Annular Mode (SAM).
- 10 • Negative SAM response to sea-ice loss damps but does not fully offset the positive SAM
11 response to increased CO₂.
- 12 • Sea-ice loss causes near-surface warming over the high-latitude Southern Ocean, but
13 warming does not penetrate the Antarctic continent.

14 **Abstract**

15 Antarctic sea-ice cover is projected to significantly decrease by the end of the 21st century if
16 greenhouse gas concentrations continue to rise, with potential consequences for Southern
17 Hemisphere weather and climate. Here, we examine the atmospheric response to projected
18 Antarctic sea-ice loss at quadrupled CO₂, inferred from eleven CMIP5 models. Our study is the
19 first multi-model analysis of the atmospheric response to Antarctic sea-ice loss. Projected sea-ice
20 loss enhances the negative phase of the Southern Annular Mode (SAM), which slightly damps
21 the positive SAM response to increased CO₂, particularly in spring. The negative SAM response
22 largely reflects a weakening of the eddy-driven jet, and to a lesser extent, an equatorward shift of
23 the jet. Sea-ice loss induces near-surface warming over the high-latitude Southern Ocean, but
24 warming does not penetrate over the Antarctic continent. In spring, we find multi-model
25 evidence for a weakened polar stratospheric vortex in response to sea-ice loss.

26 **Plain Language Summary**

27 Increasing greenhouse gases through human activities are predicted to cause a decrease in
28 Antarctic sea-ice cover by the end of the century. If this happens, it is unknown what the impacts
29 on Southern Hemisphere weather and climate could be. The aim of this study was to use
30 simulations from eleven climate models to explore the potential consequences of future Antarctic
31 sea-ice loss. We analyzed model simulations with CO₂ quadrupled from pre-industrial levels,
32 which led to large reductions in Antarctic sea-ice. We found that sea-ice loss led to warmer
33 temperatures in the lowermost atmosphere over the Southern Ocean, but that this warming did
34 not penetrate the Antarctic continent. Sea-ice loss also had an impact on the predominantly
35 westerly winds that encircle Antarctica, causing them to weaken. Climate models have some

36 difficulties in representing Antarctic sea ice, and as a result, projections of Antarctic sea ice are
37 highly uncertain. Our results imply that reducing uncertainties in projections of Antarctic sea ice
38 may lead to better forecasts of future changes in Southern Hemisphere weather and climate.

39

40 **1. Introduction**

41 Accurate satellite records of polar sea ice began in 1979. Since this time, annual-mean Arctic sea
42 ice extent (SIE) has decreased significantly by ~960 thousand square kilometers per decade
43 (Fetterer et al., 2017), whereas annual-mean Antarctic SIE has increased by a lower, but still
44 significant, ~54 thousand square kilometers per decade (Fetterer et al., 2017). In austral spring
45 2016, Antarctic SIE decreased at an abnormal rate, 18% quicker than in any previous melting
46 season in the satellite record and 46% quicker than the average melt rate (Turner et al., 2017).
47 Possible explanations for the sudden 2016 decline include influences from the El Niño Southern
48 Oscillation (ENSO) and an enhanced zonal wavenumber-3 pattern of the westerly jet (Schlosser
49 et al., 2017; Stuecker et al., 2017). In addition, new research has shown that the rapid sea-ice loss
50 led to ocean warming and enhanced upward propagation of planetary scale waves, triggering a
51 stratospheric warming event, subsequently influencing the westerly jet and further enhancing ice
52 melt (Meehl et al., 2019; Wang et al., 2019). Since 2016, Antarctic SIE has tracked well below
53 its long-term average. It is unclear if this dramatic reduction is temporary or if the Southern
54 Hemisphere sea ice is entering a new era of decline (Ludescher et al., 2018).

55

56 The Coupled Model Intercomparison Project Phase 5 (CMIP5) climate models simulate, on
57 average, a loss of sea ice over the historical period and not an increase as has been observed.
58 This disagreement between observations and models remain poorly understood (Turner et al.,
59 2013), but possible explanations include internal climate variability (Polvani & Smith, 2013),
60 model biases (e.g Bracegirdle et al., 2013; Bracegirdle et al., 2018; Holland et al., 2017; Lecomte
61 et al., 2016; Purich et al., 2016; Roach et al., 2018; Schroeter et al., 2017; Turner et al., 2013) or
62 unresolved processes in models such as ice-sheet-ocean interactions. The same models project

63 that Antarctic sea ice will continue to decline significantly by 2100 (e.g. Collins et al., 2013;
64 Vaughan, 2013) if greenhouse gas concentrations continue to rise, although there is significant
65 divergence between models in the magnitude of the projected decline. Nevertheless, future trends
66 in Antarctic sea ice may have numerous impacts on the surrounding atmosphere.

67

68 It is well understood that Arctic sea-ice loss is influencing high latitude weather and climate in
69 the Northern Hemisphere, with thermodynamically induced warming and moistening of the
70 atmosphere, amongst other changes. There is also emerging evidence that reduced Arctic sea ice
71 may influence the large-scale atmospheric circulation, for example, through weakening of the
72 mid-latitude westerly winds (e.g., Peings & Magnusdottir, 2014) and a negative shift in the North
73 Atlantic Oscillation index (Blackport & Kushner, 2016; Deser et al., 2015; Kim et al., 2014;
74 Peings & Magnusdottir, 2014; Screen & Simmonds, 2013; Screen et al., 2013). Several review
75 papers have been published on the atmospheric response to Arctic sea-ice loss, including Cohen
76 et al. (2014), Vavrus (2018) and Screen et al. (2018). The potential for such atmospheric
77 responses to Antarctic sea-ice loss has been less well studied.

78

79 The observed gradual growth of Antarctic sea ice has been suggested to result in a slight
80 poleward shift of the tropospheric jet in the austral winter months (Smith et al., 2017). Raphael et
81 al. (2011) suggested that negative summer sea ice anomalies were linked to a more negative
82 Southern Annular Mode (SAM) index and vice versa. Studies examining the atmospheric
83 response to projected Antarctic sea-ice loss have revealed contrasting results, with Kidston et al.
84 (2011) finding no significant impacts whereas Bader et al. (2013) and Menéndez et al. (1999)
85 both found an equatorward shift of the tropospheric jet. More recently, England et al. (2018)

86 used the WACCM4 model to compare impacts of Arctic and Antarctic sea-ice loss. These
87 authors found a significant equatorward shift of the eddy-driven jet in response to sea-ice loss in
88 either hemisphere. They also found that the tropospheric and stratospheric responses to Antarctic
89 sea-ice loss were of smaller amplitude, more vertically confined and with less seasonal variation
90 than in response to Arctic sea-ice loss.

91
92 In this paper, we use the CMIP5 multi-model ensemble to assess the atmospheric response to
93 projected Antarctic sea-ice loss across the Southern Hemisphere. Our study is the first to look at
94 the impacts of projected Antarctic sea-ice loss using a multi-model ensemble.

95

96 **2. Data and Methods**

97 Zappa et al. (2018) introduced a novel method of estimating the response to projected sea-ice
98 loss using existing CMIP5 simulations. Their study applied this method to analyze the
99 wintertime atmospheric response to projected Arctic sea-ice loss and in particular, that of the
100 North Atlantic jet. Here, we apply a very similar methodology to examine the seasonal
101 atmospheric response to Antarctic sea-ice loss when the CO₂ concentration is quadrupled. We
102 use output from 11 climate models (Table S4), which had all the required experiments. Prior to
103 analysis and to facilitate averaging across models, data were interpolated onto a T42 grid.

104

105 To estimate the coupled climate response to quadrupled CO₂, we compare 100-year means (years
106 50-150) from the CMIP5 ‘abrupt4xCO2’ simulations to 100-year climatologies from the
107 preindustrial control simulations (‘piControl’). We chose to use ‘abrupt4xCO2’ rather than any
108 of the Representative Concentration Pathway (RCP) experiments (Zappa et al. (2018) used

109 RCP8.5), to avoid the complicating influences of non-CO₂ climate drivers, such as ozone and
 110 aerosols, which are included in the RCPs but not in ‘abrupt4xCO₂’. Furthermore, the use of
 111 ‘abrupt4xCO₂’ results in scaling factors (described below) closer to unity, which reduces our
 112 reliance on the assumption of linear scalability of the atmospheric response to SST warming and
 113 CO₂ increase. The atmospheric response to quadrupled CO₂ was estimated by comparing 30-year
 114 means (years 1979-2008) from the ‘amip4xCO₂’ simulations to those in the ‘amip’ simulations.
 115 Likewise, the atmospheric response to SST warming was estimated by comparing 30-year means
 116 from the ‘amipFuture’ and ‘amip’ simulations. The ‘amip’ simulations were prescribed with
 117 observed variability in sea ice concentrations, sea surface temperatures (SST) and atmospheric
 118 composition for the period 1979-2008. The ‘amipFuture’ simulations are identical to ‘amip’,
 119 except that they have added SST perturbations derived from the CMIP3 ‘abrupt4xCO₂’ multi-
 120 model response, scaled to have a global average warming of 4 K. The ‘amip4xCO₂’ simulations
 121 are identical to ‘amip’ except that the CO₂ concentration was quadrupled. Sea ice is kept
 122 unchanged at present day values in both ‘amip4xCO₂’ and ‘amipFuture’, so is identical to that in
 123 ‘amip’. The fact that sea ice is unchanged, but that either SST or CO₂ is changed, allows for the
 124 response to sea-ice loss to be estimated as the residual between the coupled climate response
 125 (‘abrupt4xCO₂’ minus ‘piControl’) and the combined and scaled atmospheric responses to SST
 126 warming and quadrupled CO₂, termed $AMIP_{sst+co2}$, where:

127

$$128 \quad AMIP_{sst+co2} - AMIP = k_{sst} \cdot (AMIP_{Future} - AMIP) + k_{co2} \cdot (AMIP_{4xCO2} - AMIP) \quad (1)$$

129

130 Here, k_{sst} is the temperature scaling factor derived as the ratio of tropical 30°S-30°N zonal-mean
 131 warming at 100-300 hPa in ‘amipFuture’ (relative to ‘amip’) to that in ‘abrupt4xCO₂’ (relative

132 to ‘piControl’). This scaling was chosen to capture the tropical upper tropospheric warming,
 133 which is a dominant feature (or ‘fingerprint’) of global warming. k_{sst} was calculated for each of
 134 the eleven models, with an average of $k_{sst} = 0.8047$. k_{co2} is the scaling of CO₂ radiative
 135 forcing, which, for our purposes is unity. Hereafter we refer to the multi-model-mean difference
 136 between the coupled climate response and $AMIP_{sst+co2}$, as the inferred response to sea-ice loss.
 137 Our estimate of the inferred response to sea-ice loss is derived as a residual from coupled model
 138 experiments and so, it includes any effects of ocean coupling on the response to sea-ice loss (see,
 139 e.g., Deser et al., 2015). However due to the scaling (k_{sst}), we expect that any tropical response
 140 to sea-ice loss, and any feedback of sea-ice-induced tropical changes on the extratropics, would
 141 be missed by our method and instead apportioned to SST change.

142

143 The tropospheric eddy-driven jet shift was calculated using a monthly-mean jet latitude index
 144 (Ceppi et al., 2018; Zappa et al., 2018). The zonal average of the monthly-mean climatological
 145 zonal wind (\bar{u}) at 850hPa was first taken for the Southern Ocean. The jet latitude (ϕ_{jet}) was then
 146 defined as the mean latitude (ϕ) of westerlies weighted by the square of the westerly wind speed:

147

$$148 \quad \phi_{jet} = \int_{-30^{\circ}}^{-65^{\circ}} \phi \bar{u}_0^2 d\phi / \int_{-30^{\circ}}^{-65^{\circ}} \bar{u}_0^2 d\phi \quad (2)$$

$$149 \quad \bar{u}_0(\phi) = \max(0, \bar{u}(\phi)) \quad (3)$$

150

151 Unless otherwise stated, we use the shorthand ‘jet’ to refer to the tropospheric eddy-driven jet.
 152 We define a robust response to be when nine or more of the eleven models have the same signed
 153 response as the multimodel mean.

154

155 **3. Results**

156 In response to quadrupled CO₂, Antarctic sea ice concentrations are reduced in all seasons and in
157 all sectors of the Southern Ocean (Figure 1a-d). During the warmer months, sea-ice loss is
158 mostly limited to high southern latitudes, particularly the Weddell and Ross Seas. In the colder
159 months, sea ice reductions are simulated all around Antarctica and extend further to the north,
160 reaching 55 °S in the Atlantic sector. The loss of sea ice is of greatest magnitude in the late
161 austral autumn through to summer (May-December) and of weaker magnitude in the late austral
162 summer and early autumn (January-April). The loss of sea-ice area (Figure 1e) is greatest in
163 September ($7.7 \times 10^6 \text{ km}^2$) and least in February ($1.6 \times 10^6 \text{ km}^2$).

164

165 As would be expected, the loss of sea-ice leads to an increase in the ocean-to-atmosphere heat
166 flux at the ocean surface. Figure 1f shows the area-weighted surface turbulent (sensible plus
167 latent) heat flux response, summed over Southern Hemisphere grid points where the sea-ice
168 concentration differs between the preindustrial and quadrupled CO₂ states. The inferred heat flux
169 response to the sea-ice loss (Figure 1f) is largest in the austral winter (July-September), reaching
170 a maximum of 300 TW in August, and smallest in spring to summer, with a minimum of 50 TW
171 in January. The annual cycle of the surface heat flux response closely follows the annual cycle of
172 sea-ice area loss; although the monthly maximum and minimum heat flux responses occur one
173 month prior to the maximum and minimum sea-ice area loss. The heat flux response peaks in
174 August, despite sea-ice loss being largest in August-September, because the climatological heat
175 flux is at a maximum in July-August (not shown).

176

177 Near-surface air temperatures are significantly increased in regions of sea ice loss (Figure 2a-d),
178 consistent with an enhanced ocean-to-atmosphere heat flux. The seasons and geographical
179 regions of greatest warming are consistent with both the magnitude of sea-ice loss and of the
180 surface heat flux response. Warming reaches a maximum of 7.2 K in the Amundsen Sea in
181 austral winter. The near-surface warming does not extent far inland, probably due to the high
182 elevation of the Antarctic continent and predominantly down-slope winds, in agreement with
183 England et al. (2018).

184
185 The inferred mean surface level pressure (MSLP) response to sea-ice loss (Figure 2e-h)
186 resembles the spatial pattern of the negative phase of the SAM, with increased MSLP at high
187 latitudes and reduced MSLP in mid-latitudes, particularly in the austral spring and summer. An
188 increase in MSLP is simulated over the Antarctic continent in all seasons. The MSLP response is
189 highly zonally symmetric in spring and summer. In winter, and to a lesser extent in autumn, the
190 ring of reduced MSLP in midlatitudes is punctuated by increased MSLP in the East Pacific
191 sector (i.e., south of Australia and New Zealand). Also, in winter, MSLP is increased in the
192 Amundsen-Bellingshausen Sea, which implies a reduction in the intensity of the Amundsen Sea
193 Low. The inferred response of the westerly wind in the mid-troposphere (500 hPa; Figure 2i-l) is
194 best described as decrease in westerly wind velocity around Antarctica centered at 65 °S and an
195 increase in mid-latitudes centered at 45 °S. This general pattern is simulated in all seasons but is
196 of greatest magnitude in austral spring and summer, consistent with the MSLP response.

197
198 Figure 3a-d shows the vertical profile of the inferred zonal-mean air temperature response to sea-
199 ice loss. The near-surface warming previously discussed is confined to the lower troposphere,

200 below 500 hPa. The most notable features of the temperature response aloft are general cooling
201 of the stratosphere across a range of latitudes and seasons, and polar stratospheric warming in
202 austral spring. We suspect the former may be an artifact of method as both SST warming and
203 quadrupled CO₂ favor a cooler stratosphere (not shown). The polar stratospheric warming in
204 spring, however, is not seen in the response to either SST warming or quadrupled CO₂ and may
205 indicate a weakened stratospheric polar vortex in response to sea-ice loss.

206

207 The inferred zonal-mean westerly wind response to sea-ice loss (Figure 3e-h) shows a weakening
208 of the westerly wind at 60 °S, on the poleward flank of the eddy-driven jet, from the surface to
209 the mid-stratosphere in all seasons, but of largest magnitude in austral winter and spring. The
210 weakening of the stratospheric westerly wind at 60 °S is largest in spring and again, suggests a
211 weakened stratospheric polar vortex. In October, the models depict a robust slowdown of
212 stratospheric polar vortex by 4.5 ms⁻¹ (~10% of the climatological SPV strength in this month;
213 Figure S3). Throughout the year, but to a lesser degree in autumn, there is strengthened westerly
214 wind at 40 °S, predominantly in the core of the subtropical jet. The tropospheric response is
215 largest when there is a coincident and same-signed stratosphere response, suggesting
216 troposphere-stratosphere coupling. This result is in accordance with previous studies that have
217 suggested increased stratosphere-troposphere coupling in the austral spring when the
218 stratospheric polar vortex breaks down (e.g., Kidston et al., 2015).

219

220 Figures 2 and 3 suggest changes in the westerly eddy-driven jet in response to sea-ice loss, which
221 can be better quantified using the jet latitude and jet strength metrics. The inferred eddy-driven
222 jet latitude response (Figure 4a) shows an equatorward shift in August to February, of 1.5 °

223 latitude at its maximum in December. December and April are the only months when eight
224 models agree on the sign of the jet latitude response, with approximately seven or fewer models
225 agreeing on the sign of the response in other calendar months. The eddy-driven jet strength is
226 decreased from August to December, with the biggest reduction in jet strength of 0.75 ms^{-1} found
227 in November and corroborated by 9 models (Figure 4b). Changes in the SAM index mimic those
228 of jet strength (Figure S3). The simplest dynamical explanation for the eddy-driven jet
229 weakening is the reduction in the near-surface temperature gradient and resultant decreased
230 baroclinicity (Kidston et al., 2011). We note that the jet responses to sea-ice loss are small and,
231 in most months, of opposite sign, compared to those simulated in response to SST and CO_2 . The
232 jet strength and in particular, jet latitude responses are less robust than the 500 hPa westerly wind
233 and zonal-mean zonal wind responses described earlier. We posit that more varied jet responses
234 reflect differences in the average latitude of the jet across the models. Models with a more
235 southerly located jet tend to simulate a poleward-shifted jet in response to sea-ice loss, whereas
236 those with a more northerly located jet tend to simulate an equatorward-shifted jet in response to
237 sea-ice loss (Figure 4c). The models that depict a strengthening jet in response to sea-ice loss
238 have their jets too far north, at around 40°S , at latitudes where the westerly wind increases
239 (Figure 3). The zonal-mean westerly wind decrease is largest at 60°S (Figure 3), poleward of the
240 mean jet, and thus, the models with more poleward-located jets are also those that simulate the
241 largest reductions in jet strength in response to sea-ice loss (Figure 4d). These relationships are
242 strongest in winter and spring (not shown for other seasons) and are reminiscent of similar
243 dependencies seen for the projected jet response to increased greenhouse gas concentrations
244 (e.g., Kidston and Gerber, 2010; Bracegirdle et al., 2018).

245

246 4. Discussion

247 Our results suggest an overall weakening of the eddy-driven jet and negative shift in the SAM
248 index in response to projected Antarctic sea-ice loss, particularly in austral spring. This result is
249 in broad agreement with past studies using individual models (Bader et al., 2013; England et al.,
250 2018; Menéndez et al., 1999; Raphael et al., 2011; Smith et al., 2017), but we are the first to
251 provide evidence from a multi-model ensemble. The weakening of the eddy-driven jet and
252 negative SAM in response to sea-ice loss counteract, but only partially offset, the projected jet
253 strengthening and positive SAM in response to increased CO₂ (Figure S1, S2). Thus, projected
254 sea-ice loss acts to slightly weaken the jet and SAM response to increased CO₂. We have shown
255 that the SAM response to projected sea-ice loss primarily reflects changes in eddy-driven jet
256 strength and to a lesser extent, changes in jet latitude, consistent with England et al. (2018).

257

258 Our results suggest that in many respects, the multi-model-mean response to projected Antarctic
259 sea-ice loss is analogous to that in response to projected Arctic sea-ice loss. Consistent features
260 of the multi-model responses to Arctic and Antarctic include the weakening of the eddy-driven
261 jet, shift towards the negative phase of the annular mode, and weakening of the stratospheric
262 polar vortex, albeit with some differences in seasonality as also noted by England et al. (2018)
263 for one model. One difference between our results and that for the multi-model-mean response to
264 projected Arctic sea-ice loss is that near-surface temperature response to Antarctic sea-ice loss
265 does not extend over the Antarctic continent (Fig. 2), whereas the surface temperature response
266 to Arctic sea-ice loss does spread to the northern high-latitude continents (e.g., Zappa et al.,
267 2018). We speculate the high elevation of Antarctica isolates the continent from the low-level
268 sea-ice-induced warming. In contrast, Krinner et al. (2014) found a large temperature response

269 over the continent in atmosphere-only simulations with prescribed changes in sea ice and SST.
270 This implies that broader SST warming is key to warming over the Antarctic plateau.

271
272 Our results suggest a different seasonality to the stratospheric response to projected Antarctic
273 sea-ice loss to that in England et al. (2018). We found a robust multi-model-mean weakening of
274 the stratospheric zonal wind only in spring, whereas in the single model experiments of England
275 et al. (2018), the stratospheric zonal wind was weakened in autumn and winter, but not in spring.
276 The seasonal timing of maximum stratospheric response shown here is more in line with that in
277 response to projected Arctic sea-ice loss. In the Northern Hemisphere, sea-ice loss appears to
278 enhance the upward propagation of planetary scales waves causing a weakening of the polar
279 vortex in late winter or spring (e.g., Kim et al., 2014). However, it is unclear whether this
280 mechanism operates in the Southern Hemisphere and the zonal symmetry of multi-model-mean
281 tropospheric circulation response implies only small changes in upward wave propagation.
282 Further work with dedicated sea-ice perturbation experiments is required to understand the
283 origins of the stratospheric response to Antarctic sea-ice loss.

284

285

286 **5. Conclusions**

287 We have undertaken the first multi-model analysis of the atmospheric response to projected
288 Antarctic sea-ice loss. We find some robust aspects of the atmospheric circulation response to
289 sea-ice loss across eleven models, despite large differences between the models in many aspects.
290 Our results suggest that projected sea-ice loss causes a robust weakening of the tropospheric
291 westerly jet and favors the negative phase of the SAM, of greatest magnitude and robustness in

292 austral spring and summer. In these regards, the response to sea-ice loss acts to weakly damp the
293 strengthening westerly jet and positive SAM responses to increased CO₂. We have shown that
294 the SAM response to sea-ice loss primarily reflects a reduction in jet strength and to a lesser
295 extent, an equatorward shift in the jet. In austral spring, we find multi-model evidence for a
296 weakening polar stratospheric vortex and coupling between the stratospheric and tropospheric
297 zonal wind responses. Sea-ice loss induces warming in the lowermost atmosphere over the high-
298 latitude Southern Ocean, but this warming does not penetrate over the Antarctic continent.

299

300 **Acknowledgments, Samples, and Data**

301 We thank Thomas Bracegirdle for useful discussions and for commenting on an earlier draft of
302 the paper. We acknowledge the World Climate Research Programme Working Group on
303 Coupled Modelling, which is responsible for CMIP, and the modeling groups listed in Table S1
304 for producing the simulations and making available their output. CMIP data were obtained from
305 the British Atmospheric Data Centre. This study is supported by the “Robust Spatial Projections
306 of Real-World Climate Change” (NERC, Research grant NE/N018486/1) and the University of
307 Exeter.

308

309 **Figure captions**

310 Multi-model-mean sea ice concentration response to quadrupled CO₂ in austral (a) summer
311 (January-March; JFM), (b) autumn (April-June; AMJ), (c) winter (July-September; JAS) and (d)
312 spring (October-December). The black and grey contours show the sea-ice edge (15%
313 concentration) in the quadrupled and control simulations, respectively. (e) Multi-model-mean
314 sea-ice area (SIA) response to quadrupled CO₂ as a function of calendar month. The right-hand

315 vertical axis (in blue) shows the number of models that have the same signed response as the
316 multimodel mean, with filled dots indicating nine or more models have the same signed response
317 as the multimodel mean and stars indicating fewer than nine models have the same signed
318 response as the multimodel mean. (f) As (e), but for the inferred surface turbulent heat flux
319 response, calculated as the area-weighted surface turbulent (sensible plus latent) heat flux
320 response, summed over Southern Hemisphere grid points where the sea-ice concentration differs
321 between the preindustrial and quadrupled CO₂ states. The heat flux is defined as positive in the
322 upward direction.

323
324 Figure 2: Multi-model-mean inferred surface air temperature (TAS) response to Antarctic sea-ice
325 loss in austral (a) summer (January-March; JFM), (b) autumn (April-June; AMJ), (c) winter
326 (July-September; JAS) and (d) spring (October-December). In areas enclosed by the grey
327 contours nine or more models have the same signed response as the multimodel mean. (e-h) As
328 (a-d), but for mean sea level pressure (MSLP). (i-l) As (a-d), but for 500 hPa westerly wind
329 (U500). The thick black line represents the climatological jet position.

330
331 Figure 3: Multi-model-mean inferred zonal-mean air temperature response to Antarctic sea-ice
332 loss in austral (a) summer (January-March; JFM), (b) autumn (April-June; AMJ), (c) winter
333 (July-September; JAS) and (d) spring (October-December). The black contours show the
334 baseline climatology and hatching indicates where nine or more models have the same signed
335 response as the multimodel mean. (e-h) As (a-d), but for zonal-mean westerly wind.

336
337 Figure 4: Multi-model-mean inferred jet latitude response to Antarctic sea-ice loss (black line)
338 and the combined response to SST and CO₂ (dashed line) as a function of calendar month. The

339 right-hand vertical axis (in blue) shows the number of individual models that have the same
340 signed response to sea-ice loss as the multi-model-mean, with filled dots indicating nine or more
341 models agree and stars indicating fewer than nine models agree. (b) As (a), but for jet strength.
342 (c) Jet latitude response to Antarctic sea-ice loss as a function of the climatological jet latitude in
343 the preindustrial control simulation for each model (crosses) and for austral winter (red) and
344 spring (black). Also shown are the linear relationships and their associated correlation
345 coefficients. (d) As (c) but for jet strength.
346

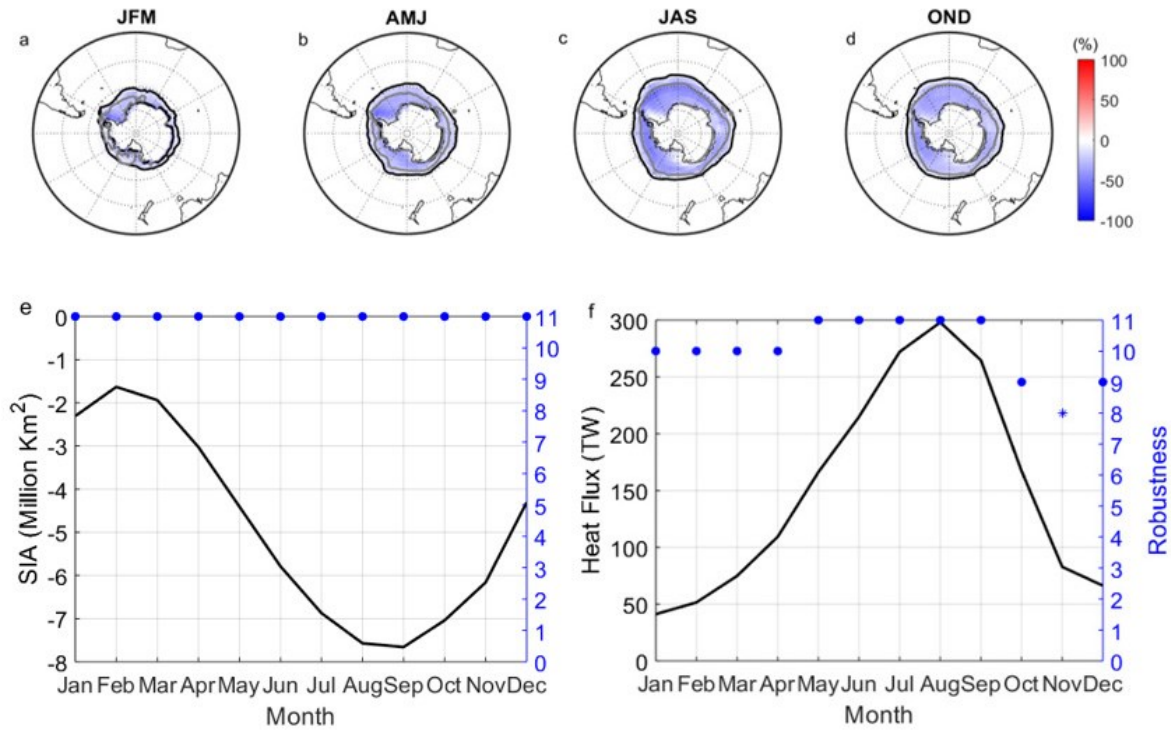
347 References

- 348 Bader, J., Flügge, M., Kvamstø, N. G., Mesquita, M. D. S., & Voigt, A. (2013). Atmospheric
349 winter response to a projected future Antarctic sea-ice reduction: A dynamical analysis.
350 *Climate Dynamics*, 40(11–12), 2707–2718. <https://doi.org/10.1007/s00382-012-1507-9>
- 351 Blackport, R., & Kushner, P. J. (2016). The transient and equilibrium climate response to rapid
352 summertime sea ice loss in CCSM4. *Journal of Climate*, 29(2), 401–417.
353 <https://doi.org/10.1175/JCLI-D-15-0284.1>
- 354 Bracegirdle, T. J., Hyder, P., & Holmes, C. R. (2018). CMIP5 Diversity in Southern Westerly Jet
355 Projections Related to Historical Sea Ice Area: Strong Link to Strengthening and Weak
356 Link to Shift. *Journal of Climate*, 31(1), 195–211. <https://doi.org/10.1175/JCLI-D-17-0320.1>
- 358 Bracegirdle, T. J., Shuckburgh, E., Sallee, J. B., Wang, Z., Meijers, A. J. S., Bruneau, N., ...
359 Wilcox, L. J. (2013). Assessment of surface winds over the atlantic, indian, and pacific
360 ocean sectors of the southern ocean in cmip5 models: Historical bias, forcing response, and
361 state dependence. *Journal of Geophysical Research Atmospheres*, 118(2), 547–562.
362 <https://doi.org/10.1002/jgrd.50153>
- 363 Ceppi, P., Zappa, G., Shepherd, T. G., & Gregory, J. M. (2018). Fast and slow components of the
364 extratropical atmospheric circulation response to CO2 forcing. *Journal of Climate*, 31(3),
365 1091–1105. <https://doi.org/10.1175/JCLI-D-17-0323.1>
- 366 Cohen, J., Screen, J. A., Furtado, J. C., Barlow, M., Whittleston, D., Coumou, D., ... Jones, J.
367 (2014). Recent Arctic amplification and extreme mid-latitude weather. *Nature Geoscience*,
368 7(9), 627–637. <https://doi.org/10.1038/ngeo2234>
- 369 Collins, M., Knutti, R., Arblaster, J., Dufresne, J.-L., Fichet, T., Friedlingstein, P., ... Wehner,
370 M. (2013). Long-term Climate Change: Projections, Commitments and Irreversibility.
371 *Climate Change 2013: The Physical Science Basis. Contribution of Working Group I to the*
372 *Fifth Assessment Report of the Intergovernmental Panel on Climate Change*, 1029–1136.
373 <https://doi.org/10.1017/CBO9781107415324.024>
- 374 Deser, C., Tomas, R. A., & Sun, L. (2015). The role of ocean-atmosphere coupling in the zonal-
375 mean atmospheric response to Arctic sea ice loss. *Journal of Climate*, 28(6), 2168–2186.
376 <https://doi.org/10.1175/JCLI-D-14-00325.1>
- 377 England, M., Polvani, L., & Sun, L. (2018). Contrasting the Antarctic and Arctic atmospheric
378 responses to projected sea ice loss in the late twenty-first century. *Journal of Climate*,
379 31(16), 6353–6370. <https://doi.org/10.1175/JCLI-D-17-0666.1>
- 380 Fetterer, F., K. Knowles, W. N. Meier, M. Savoie, and A. K. Windnagel. 2017, updated daily.
381 Sea Ice Index, Version 3.. Boulder, Colorado USA. NSIDC: National Snow and Ice Data
382 Center. doi: <https://doi.org/10.7265/N5K072F8>.
- 383 Holland, M. M., Landrum, L., Kostov, Y., & Marshall, J. (2017). Sensitivity of Antarctic sea ice
384 to the Southern Annular Mode in coupled climate models. *Climate Dynamics*, 49(5–6),
385 1813–1831. <https://doi.org/10.1007/s00382-016-3424-9>
- 386 Kidston, J., & E. P. Gerber (2010). Intermodel variability of the poleward shift of the austral jet

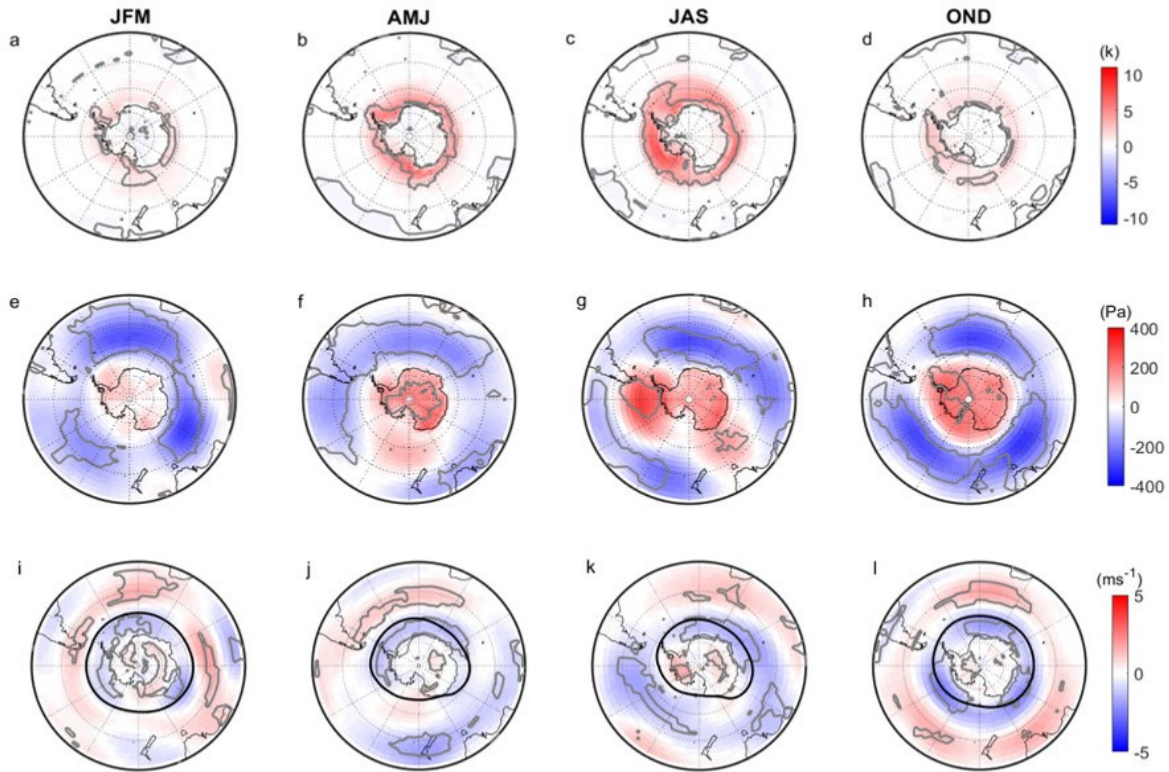
- 387 stream in the CMIP3 integrations linked to biases in 20th century climatology. *Geophys.*
388 *Res. Lett.*, **37**, L09708, doi:<https://doi.org/10.1029/2010GL042873>
- 389 Kidston, J., Taschetto, A. S., Thompson, D. W. J., & England, M. H. (2011). The influence of
390 Southern Hemisphere sea-ice extent on the latitude of the mid-latitude jet stream.
391 *Geophysical Research Letters*, 38(15), 1–5. <https://doi.org/10.1029/2011GL048056>
- 392 Kidston, J., Scaife, A. A., Hardiman, S. C., Mitchell, D. M., Butchart, N., Baldwin, M. P., &
393 Gray, L. J. (2015). Stratospheric influence on tropospheric jet streams, storm tracks and
394 surface weather. *Nature Geoscience*, 8(6), 433–440. <https://doi.org/10.1038/NGL0424>
- 395 Kim, B. M., Son, S. W., Min, S. K., Jeong, J. H., Kim, S. J., Zhang, X., ... Yoon, J. H. (2014).
396 Weakening of the stratospheric polar vortex by Arctic sea-ice loss. *Nature Communications*,
397 5, 1–8. <https://doi.org/10.1038/ncomms5646>
- 398 Krinner, G., Langeron, C., Ménégoz, M., Agosta, C., & Brutel-Vuilmet, C. (2014). Oceanic
399 forcing of Antarctic climate change: A study using a stretched-grid atmospheric general
400 circulation model. *Journal of Climate*, 27(15), 5786–5800. [https://doi.org/10.1175/JCLI-D-](https://doi.org/10.1175/JCLI-D-13-00367.1)
401 13-00367.1
- 402 Lecomte, O., Goosse, H., Fichefet, T., Holland, P. R., Uotila, P., Zunz, V., & Kimura, N. (2016).
403 Impact of surface wind biases on the Antarctic sea ice concentration budget in climate
404 models. *Ocean Modelling*, 105, 60–70. <https://doi.org/10.1016/j.ocemod.2016.08.001>
- 405 Ludescher, J., Yuan, N., & Bunde, A. (2018). Detecting the statistical significance of the trends
406 in the Antarctic sea ice extent: an indication for a turning point. *Climate Dynamics*, 53(1),
407 237–244. <https://doi.org/10.1007/s00382-018-4579-3>
- 408 Meehl, G. A., Arblaster, J. M., Chung, C. T. Y., Holland, M. M., DuVivier, A., Thompson, L.,
409 ... Bitz, C. M. (2019). Sustained ocean changes contributed to sudden Antarctic sea ice
410 retreat in late 2016. *Nature Communications*, 10(1), 14. [https://doi.org/10.1038/s41467-018-](https://doi.org/10.1038/s41467-018-07865-9)
411 07865-9
- 412 Menéndez, C. G., Serafini, V., & Le Treut, H. (1999). The effect of sea-ice on the transient
413 atmospheric eddies of the Southern Hemisphere. *Climate Dynamics*, 15(9), 659–671.
414 <https://doi.org/10.1007/s003820050308>
- 415 Peings, Y., & Magnusdottir, G. (2014). Response of the wintertime northern hemisphere
416 atmospheric circulation to current and projected arctic sea ice decline: A numerical study
417 with CAM5. *Journal of Climate*, 27(1), 244–264. [https://doi.org/10.1175/JCLI-D-13-](https://doi.org/10.1175/JCLI-D-13-00272.1)
418 00272.1
- 419 Polvani, L. M., & Smith, K. L. (2013). Can natural variability explain observed Antarctic sea ice
420 trends? New modeling evidence from CMIP5. *Geophysical Research Letters*, 40(12), 3195–
421 3199. <https://doi.org/10.1002/grl.50578>
- 422 Purich, A., Cai, W., England, M. H., & Cowan, T. (2016). Evidence for link between modelled
423 trends in Antarctic sea ice and underestimated westerly wind changes. *Nature*
424 *Communications*, 7(May 2015), 10409. <https://doi.org/10.1038/ncomms10409>
- 425 Raphael, M. N., Hobbs, W., & Wainer, I. (2011). The effect of Antarctic sea ice on the Southern
426 Hemisphere atmosphere during the southern summer. *Climate Dynamics*, 36(7), 1403–
427 1417. <https://doi.org/10.1007/s00382-010-0892-1>

- 428 Roach, L. A., Dean, S. M., & Renwick, J. A. (2018). Consistent biases in Antarctic sea ice
429 concentration simulated by climate models. *Cryosphere*, 12(1), 365–383.
430 <https://doi.org/10.5194/tc-12-365-2018>
- 431 Schlosser, E., Haumann, F. A., & Raphael, M. N. (2017). Atmospheric influences on the
432 anomalous 2016 Antarctic sea ice decay. *The Cryosphere Discussions*, 13(3), 1–31.
433 <https://doi.org/10.5194/tc-2017-192>
- 434 Schroeter, S., Hobbs, W., & Bindoff, N. L. (2017). Interactions between Antarctic sea ice and
435 large-scale atmospheric modes in CMIP5 models. *The Cryosphere*, 11(2), 789–803.
436 <https://doi.org/10.5194/tc-11-789-2017>
- 437 Screen, James A., Deser, C., Smith, D. M., Zhang, X., Blackport, R., Kushner, P. J., ... Sun, L.
438 (2018). Consistency and discrepancy in the atmospheric response to Arctic sea-ice loss
439 across climate models. *Nature Geoscience*, 11(3), 155–163. [https://doi.org/10.1038/s41561-](https://doi.org/10.1038/s41561-018-0059-y)
440 [018-0059-y](https://doi.org/10.1038/s41561-018-0059-y)
- 441 Screen, James A., & Simmonds, I. (2013). Exploring links between Arctic amplification and
442 mid-latitude weather. *Geophysical Research Letters*, 40(5), 959–964.
443 <https://doi.org/10.1002/grl.50174>
- 444 Screen, James A., Simmonds, I., Deser, C., & Tomas, R. (2013). The atmospheric response to
445 three decades of observed arctic sea ice loss. *Journal of Climate*, 26(4), 1230–1248.
446 <https://doi.org/10.1175/JCLI-D-12-00063.1>
- 447 Smith, D. M., Dunstone, N. J., Scaife, A. A., Fiedler, E. K., Copsey, D., & Hardiman, S. C.
448 (2017). Atmospheric response to Arctic and Antarctic sea ice: The importance of ocean-
449 atmosphere coupling and the background state. *Journal of Climate*, 30(12), 4547–4565.
450 <https://doi.org/10.1175/JCLI-D-16-0564.1>
- 451 Stuecker, M. F., Bitz, C. M., & Armour, K. C. (2017). Conditions leading to the unprecedented
452 low Antarctic sea ice extent during the 2016 austral spring season. *Geophysical Research*
453 *Letters*, 1–12. <https://doi.org/10.1002/2017GL074691>
- 454 Turner, J., Bracegirdle, T. J., Phillips, T., Marshall, G. J., & Scott Hosking, J. (2013). An initial
455 assessment of antarctic sea ice extent in the CMIP5 models. *Journal of Climate*, 26(5),
456 1473–1484. <https://doi.org/10.1175/JCLI-D-12-00068.1>
- 457 Turner, J., Phillips, T., Marshall, G. J., Hosking, J. S., Pope, J. O., Bracegirdle, T. J., & Deb, P.
458 (2017). Unprecedented springtime retreat of Antarctic sea ice in 2016. *Geophysical*
459 *Research Letters*, 44(13), 6868–6875. <https://doi.org/10.1002/2017GL073656>
- 460 Vaughan, D. G. J. C. C. (2013). Observations: Cryosphere. *Climate Change 2013 the Physical*
461 *Science Basis: Working Group I Contribution to the Fifth Assessment Report of the*
462 *Intergovernmental Panel on Climate Change*, 9781107057, 317–382.
463 <https://doi.org/10.1017/CBO9781107415324.012>
- 464 Vavrus, S. J. (2018). The Influence of Arctic Amplification on Mid-latitude Weather and
465 Climate. *Current Climate Change Reports*, 4(3), 238–249. [https://doi.org/10.1007/s40641-](https://doi.org/10.1007/s40641-018-0105-2)
466 [018-0105-2](https://doi.org/10.1007/s40641-018-0105-2)
- 467 Wang, G., Hendon, H. H., Arblaster, J. M., Lim, E.-P., Abhik, S., & van Rensch, P. (2019).
468 Compounding tropical and stratospheric forcing of the record low Antarctic sea-ice in 2016.

469 Nature Communications, 10(1), 13. <https://doi.org/10.1038/s41467-018-07689-7>
470 Zappa, G., Pithan, F., & Shepherd, T. G. (2018). Multimodel Evidence for an Atmospheric
471 Circulation Response to Arctic Sea Ice Loss in the CMIP5 Future Projections. *Geophysical*
472 *Research Letters*, 45(2), 1011–1019. <https://doi.org/10.1002/2017GL076096>

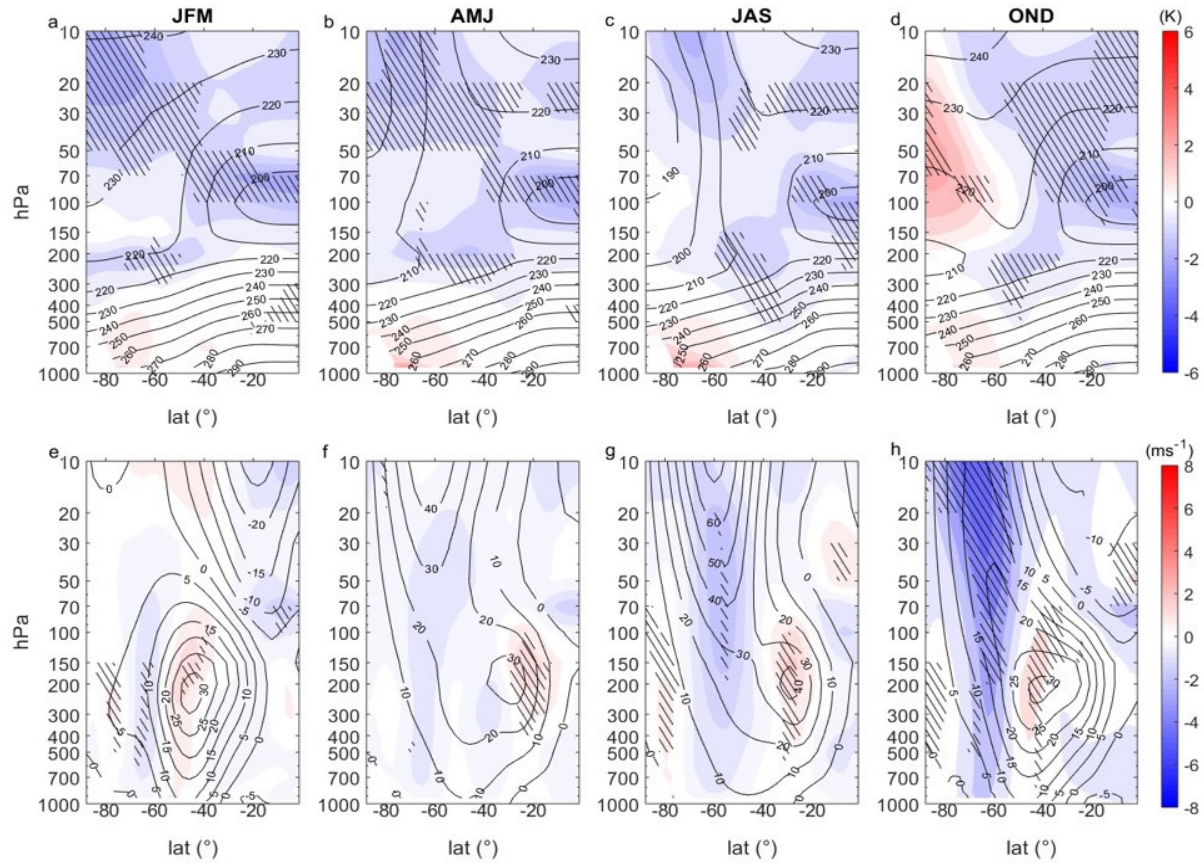


473
 474
 475 **Figure 1:** Multi-model-mean sea ice concentration response to quadrupled CO₂ in austral (a)
 476 summer (January-March; JFM), (b) autumn (April-June; AMJ), (c) winter (July-September; JAS)
 477 and (d) spring (October-December). The black and grey contours show the sea-ice edge (15%
 478 concentration) in the quadrupled and control simulations, respectively. (e) Multi-model-mean
 479 sea-ice area (SIA) response to quadrupled CO₂ as a function of calendar month. The right-hand
 480 vertical axis (in blue) shows the number of models that have the same signed response as the
 481 multimodel mean, with filled dots indicating nine or more models have the same signed response
 482 as the multimodel mean and stars indicating fewer than nine models have the same signed
 483 response as the multimodel mean. (f) As (e), but for the inferred surface turbulent heat flux
 484 response, calculated as the area-weighted surface turbulent (sensible plus latent) heat flux
 485 response, summed over Southern Hemisphere grid points where the sea-ice concentration differs
 486 between the preindustrial and quadrupled CO₂ states. The heat flux is defined as positive in the
 487 upward direction.



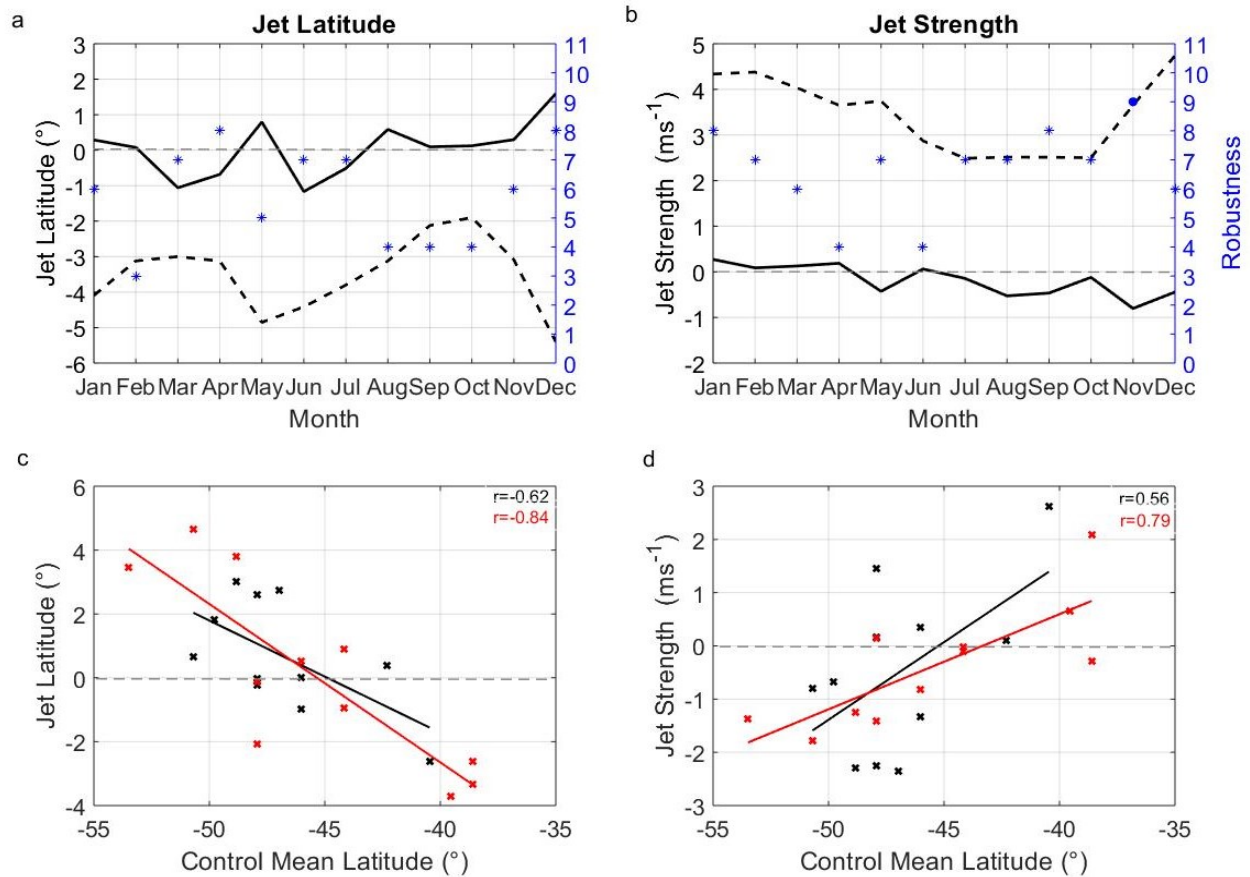
488

489 **Figure 2:** Multi-model-mean inferred surface air temperature (TAS) response to Antarctic sea-
 490 ice loss in austral (a) summer (January-March; JFM), (b) autumn (April-June; AMJ), (c) winter
 491 (July-September; JAS) and (d) spring (October-December). In areas enclosed by the grey
 492 contours nine or more models have the same signed response as the multimodel mean. (e-h) As
 493 (a-d), but for mean sea level pressure (MSLP). (i-l) As (a-d), but for 500 hPa westerly wind
 494 (U500). The thick black line represents the climatological jet position.



495
496
497

Figure 3: Multi-model-mean inferred zonal-mean air temperature response to Antarctic sea-ice loss in austral (a) summer (January-March; JFM), (b) autumn (April-June; AMJ), (c) winter (July-September; JAS) and (d) spring (October-December). The black contours show the baseline climatology and hatching indicates where nine or more models have the same signed response as the multimodel mean. (e-h) As (a-d), but for zonal-mean westerly wind.



502

503 **Figure 4:** Multi-model-mean inferred jet latitude response to Antarctic sea-ice loss (black line)504 and the combined response to SST and CO₂ (dashed line) as a function of calendar month. The

505 right-hand vertical axis (in blue) shows the number of individual models that have the same

506 signed response to sea-ice loss as the multi-model-mean, with filled dots indicating nine or more

507 models agree and stars indicating fewer than nine models agree. (b) As (a), but for jet strength.

508 (c) Jet latitude response to Antarctic sea-ice loss as a function of the climatological jet latitude in

509 the preindustrial control simulation for each model (crosses) and for austral winter (red) and

510 spring (black). Also shown are the linear relationships and their associated correlation

511 coefficients. (d) As (c) but for jet strength.

512